Design model and load reduction assessment for multi-rotational mode individual pitch control (higher harmonics control)

T.G. van Engelen

This report has been presented at the European Wind Energy Conference 2006 in Athens February 27 - March 2, 2006

MARCH 2006

Design Model and Load Reduction Assessment for Multi-rotational Mode Individual Pitch Control (Higher Harmonics Control)

T.G. van Engelen

Energy research Centre of the Netherlands (ECN), Wind Energy
P.O. Box 1, NL-1755 ZG Petten, The Netherlands
telephone: +31 224 564141, telefax: +31 224 568214
email: vanengelen@ecn.nl

ABSTRACT

A simple model has been derived for the combined design of collective and individual pitch control of 3 bladed HAWTs. Control loops were designed for a typical 3 MW variable speed wind turbine and the performance was evaluated in aero-elastic simulations. The individual pitch control reduces the loads from rotationally sampled turbulence, tower stagnation and wind shear. The involved pitching activity is centered around the rotational frequency (IPC-1p) and multiples of it (IPC-2p, IPC-3p; 'higher harmonics control'). The fatigue damage of the blades in full load is substantially reduced while one third or more is obtained from IPC-2p and IPC-3p; the fatigue damage reduction of the nacelle is almost completely obtained from IPC-2p. Very elementary feedback laws appear to satify when combined with de- and re-modulation schemes based on multi-blade coordinate transformations in the kp-frequencies ($k = 1, 2, 3$). This is clarified via the decomposition of the wind speed on the rotor blades in rotational modes.

KEYWORDS

Individual pitch control, Control design model, Higher Harmonics Control, Rotational Modes

1 INTRODUCTION

The loads on the rotor blades, drive-train and tower of horizontal axis wind turbines are caused for a significant part by the rotational sampling of turbulence, the tower shadow and the windshear. These loads can be reduced via individual pitch control. The earlier publications [1] and [2] give an impression of the potential of this control concept, focused on load reduction around one time the rotational frequency (IPC-1p). The method for the design of the feedback loops for individual pitch control has been explained in [2] .

However, a control design model and a model-based motivation for the choice of the structure of the feedback loops (feedback laws) as well as a model-based parametrisation of these loops have not yet been published. Besides, a drawback of the limitation to IPC-1p is the still existing blade load components around multiples of the rotational speed (2p, 3p, ...). Perhaps even more important are the loads on the nacelle around the 3p-frequency in case of a three bladed wind turbine, which is the prevailing layout. So, compensation for the higher harmonic excitation from the wind is expected to be worthwhile.

This paper presents a simple control design model that caters for the individual blade behaviour (§2). The model is used for the design of feedback loops for IPC-1p (§3); it also appears to allow for the design of feedback loops for individual pitch control around the 2p- and 3p-frequency (IPC-2p, IPC-3p. Time-domain simulations with the controlled model show the effect of IPC-kp control on the stationary blade and nacelle loads (§4).

The control design model does not include blade bending and unsteady aerodynamics. Therefore it should be considered as the first step in the development of model-based IPC-kp design. The IPC-kp loops are simultaneously active, which will cause some interaction. Stability analysis requires an integrated dynamic model, which will contain some periodic coefficients. This can be dealt with via the Floquet theory. [13] .

2 CONTROL DESIGN MODEL

The control design model pertains to a three bladed horizontal axis wind turbine ($B = 3$). The main features of the model are:

- individually pitch-controlled rigid blades;
- main rotation and 1st drive-train torsion mode;
- 1st fore-aft and sideward tower bending mode;
- controllable generator torque.

A schematic layout of the wind turbine model is pictured in Fig. 1. The model also contains three so called *blade effective* wind input signals ($\tilde{u}_1$, $\tilde{u}_2$, $\tilde{u}_3$). When such a signal acts as a uniform wind speed on the rotor blade, it causes blade root loads that are similar to those arising from a rotating blade in a wind field. A comprehensive description is in [3] .

The next two subsections deal with the linearised aerodynamic conversion behaviour for the individual rotor blades and the basic linear model equations.

2.1 Linearised aerodynamic conversion

The aerodynamic conversion is based on linearised BEM-theory; dynamic wake effects and unsteady aerodynamics are not taken into account. The BEM-based aerodynamic conversion characteristics are translated into multipliers that map a variation in the flapwise relative wind speed v_{fl_i} to variations in

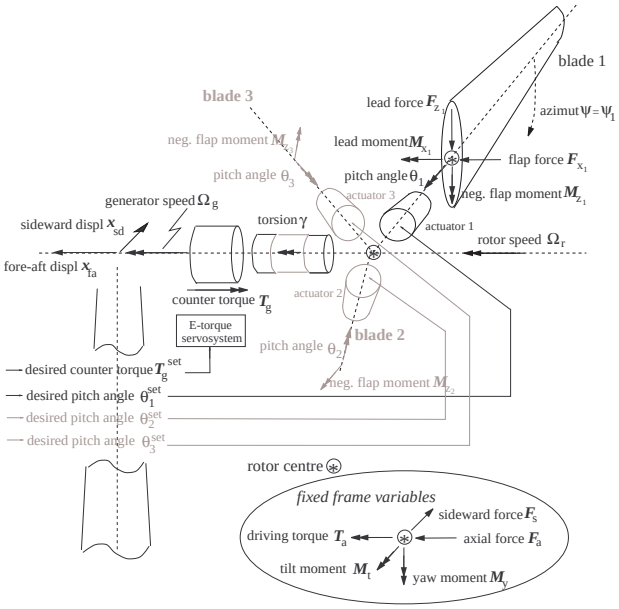

Figure 1: *Schematic layout wind turbine model*

the flap- and leadwise blade root moments and forces (aerodynamic gains). Aerodynamic gains are also derived for the linearised influcence of a variation in the pitch angle. The pitch angle variation θ_i and relative wind speed variation v_{fl_i} for the i^{th} blade thus cause variations in the aerodynamic loads on the blade root by (see fig. 1 for orientation):

$$\begin{aligned}
\delta M_{z_i} &= h_{M_z}\, v_{\mathrm{fl}_i} + k_{M_z}\, \theta_i \quad \text{(neg. flapwise moment)} \\
\delta F_{x_i} &= h_{F_x}\, v_{\mathrm{fl}_i} + k_{F_x}\, \theta_i \quad \text{(pos. flapwise force)} \\
\delta M_{x_i} &= h_{M_x}\, v_{\mathrm{fl}_i} + k_{M_x}\, \theta_i \quad \text{(pos. leadwise moment)} \\
\delta F_{z_i} &= h_{F_z}\, v_{\mathrm{fl}_i} + k_{F_z}\, \theta_i \quad \text{(pos. leadwise force)}
\end{aligned} \tag{1}$$

For variation δT_{a} in the driving torque, δF_{a} in the axial force, δM_{t} in the tilt moment and δF_{s} in the sideward force holds:

$$\begin{aligned}
\delta T_{\mathrm{a}} &= \sum_{i=1}^{B} \delta M_{x_i} \quad ; \quad \delta F_{\mathrm{a}} = \sum_{i=1}^{B} \delta F_{x_i} \\
\delta M_{\mathrm{t}} &= \sum_{i=1}^{B} \sin\psi_i\, \delta M_{z_i} \quad ; \quad \delta F_{\mathrm{s}} = -\sum_{i=1}^{B} \sin\psi_i\, \delta F_{z_i}
\end{aligned} \tag{2}$$

The flapwise relative wind speed variation v_{fl_i} for the i^{th} blade is the sum of the blade effective wind speed $\tilde{u}_i$ and the upwind motion of the rotor blade. The latter is caused by fore-aft tower bending only since rigid blades are assumed. The upwind structural motion involves both the fore-aft translation $\dot{x}_{\mathrm{fa}}$ and tilt rotation $\dot{\phi}_{\mathrm{fa}}$ of the tower top; the latter has an azimut dependent effect on the relative wind speed which varies over the rotor radius. The 3/4 blade radius location of the rotor blades ($\frac{3R_{\mathrm{b}}}{4}$) is assumed to be the effective location for taking into account $\dot{\phi}_{\mathrm{fa}}$ in the *one-point-model-approach* to blade loading. The flapwise relative wind speed v_{fl_i} is determined as:

$$v_{\mathrm{fl}_i} = \tilde{u}_i - \dot{x}_{\mathrm{fa}} + \sin(\psi_i)\, \tfrac{3}{2H}\, \tfrac{3R_{\mathrm{b}}}{4}\, \dot{x}_{\mathrm{fa}} \tag{3}$$

The multiplier $\frac{3}{2H}$ is exactly the ratio between displacement and rotation if a prismatic beam of length H is subjected to a bending force load.

At azimut angle ψ ($= \int_{-\infty}^{t} \Omega_{\mathrm{r}}(\tau)\, \mathrm{d}\tau$) equal to 0, the first blade is in the horizontal position while it is rotating downward. For the azimut angles ψ_1, ψ_2 and ψ_3 of the three blades holds:

$$\psi_1 = \psi \quad ; \quad \psi_2 = \psi + \tfrac{2}{3}\pi \quad ; \quad \psi_3 = \psi + \tfrac{4}{3}\pi \tag{4}$$

The gains $h_{M_z} \ldots k_{F_z}$ are derived from the power and thrust coefficient data in a chosen working point, characterised by wind speed, rotor speed and pitch angle. The derivation is constrained by the assumption of equal aerodynamic efficiency along the blade radius, which implies a *linear increasing* flapwise force per unit span $f_{\mathrm{fl}}(r)$ over the rotor radius and *constant* leadwise force per unit span $f_{\mathrm{ld}}(r)$.

2.2 Periodic linear model equations

The model equations that are required for controller design are the equations of motions and the output equations; the latter express the measureument variables that are input to the feedback loops in state and input variables, the 'typical' variables in the equations of motion.

Equations of motion

The variables of the drive-train are the rotor speed Ω_{r}, generator speed Ω_{g} and the shaft torsion γ; all drive-train variables are scaled to the speed level of the rotor shaft. The drive-train is accelerated by the aerodynamic driving torque T_{a} and decelerated by the generator torque T_{g}. With linear and angular fore-aft tower motion included in the relative wind speed on the rotor blades, the equations of motion for the rotor speed Ω_{r} and shaft torsion γ (eom1, eom2) become:

$$\begin{aligned}
J_{\mathrm{r}}\, \dot{\Omega}_{\mathrm{r}} &\overset{\mathrm{eom1}}{=} \delta T_{\mathrm{a}} - s_{\mathrm{sh}}\, \gamma - d_{\mathrm{sh}}\, \dot{\gamma} \\
\tfrac{J_{\mathrm{r}}\, J_{\mathrm{g}}}{J_{\mathrm{r}}+J_{\mathrm{g}}}\, \ddot{\gamma} &\overset{\mathrm{eom2}}{=} \tfrac{J_{\mathrm{g}}}{J_{\mathrm{r}}+J_{\mathrm{g}}}\, \delta T_{\mathrm{a}} - s_{\mathrm{sh}}\, \gamma - d_{\mathrm{sh}}\, \dot{\gamma} + \tfrac{J_{\mathrm{r}}}{J_{\mathrm{r}}+J_{\mathrm{g}}}\, \delta T_{\mathrm{g}}
\end{aligned} \tag{5}$$

with linearised torque variation δT_{a} by (Eq. 1 2, 3):

$$\delta T_{\mathrm{a}} = \sum_{i=1}^{B} \left[h_{M_x}\, \tilde{u}_i + k_{M_x}\, \theta_i \right] - B\, h_{M_x}\, \dot{x}_{\mathrm{fa}} \tag{6}$$

The drive-train parameters are the slow-shaft equivalent moments of inertia J_{r} and J_{g} of the rotor and generator and the stiffness and damper constant s_{sh} and d_{sh}. The values are to be tuned such that torsion behaviour agrees with the first collective lead mode; this yields a slightly underestimated moment of inertia J_{r} in the eom for Ω_{r}, which is of minor importance since this hardly affects rotor speed regulation control.

The variables of the included tower model are the fore-aft and sideward tower top displacement x_{fa} and

$x_{\rm sd}$. The fore-aft motion is driven by the thrust force $F_{\rm a}$ and aerodynamic tilt moment $M_{\rm t}$. A positive tilt moment causes upward tilting of the rotor centre, so positive fore-aft translation. The sideward motion is driven by the generator torque $T_{\rm g}$ and the sideward aerodynamic force $F_{\rm s}$. The equations of motion for fore-aft and sideward tower bending are:

$$\begin{aligned} m_{\rm tw}\,\ddot{x}_{\rm fa} &\overset{\rm eom3}{=} \delta F_{\rm a} + \tfrac{3}{2H}\,\delta M_{\rm t} - s_{\rm tw}\,x_{\rm fa} - d_{\rm tw}\,\dot{x}_{\rm fa} \\ m_{\rm tw}\,\ddot{x}_{\rm sd} &\overset{\rm eom4}{=} \tfrac{3}{2H}\,\delta T_{\rm g} + \delta F_{\rm s} - s_{\rm tw}\,x_{\rm sd} - d_{\rm tw}\,\dot{x}_{\rm sd} \end{aligned} \tag{7}$$

The multiplication factor $\frac{3}{2H}$ for the bending moment loads in the equationsof motion exactly applies if a prismatic beam is involved.

For the linearised variation in the axial force, tilt moment and sideward force holds (Eq. 1 2, 3; $\sum_{i=1}^{B}\sin^2\psi_i = \frac{1}{2}B$):

$$\begin{aligned} \delta F_{\rm a} &= \sum_{i=1}^{B}\left[h_{F_x}\,\tilde{u}_i + k_{F_x}\,\theta_i\right] - B\,h_{F_x}\,\dot{x}_{\rm fa}\ . \\ \delta M_{\rm t} &= \sum_{i=1}^{B}\sin\psi_i\,\left[h_{M_z}\,\tilde{u}_i + k_{M_z}\,\theta_i\right] + \tfrac{3}{2}\,\tfrac{9Rb}{8H}\,h_{M_z}\,\dot{x}_{\rm fa} \\ \delta F_{\rm s} &= \sum_{i=1}^{B} -\sin\psi_i\,\left[h_{F_z}\,\tilde{u}_i + k_{F_z}\,\theta_i\right] - \tfrac{3}{2}\,\tfrac{9Rb}{8H}\,h_{F_z}\,\dot{x}_{\rm fa} \end{aligned} \tag{8}$$

Equal values for the tower top equivalent mass $m_{\rm tw}$, damper constant $d_{\rm tw}$ and spring constant $s_{\rm tw}$ apply in the fore-aft and sideward equation of motion. These are based on structural data:

- horizontal tower displacement at unity force;
- damping rate of the 1st bending mode(s);
- average of the 1st fore-aft and sideward frequency.

Output equations

Next to the equations of motion, output equations apply when feedback control is considered. The individual pitch control can be realised by feedback of the blade root bending moments, the shaft bending moments or the yaw and tilt moment on the nacelle. In order to describe the approach to multi-rotational mode individual pitch control as straightforward as possible, we choose the feedback of the blade root bending moment variations δM_{z_i}. It holds (oe1 means 1st output equation, etc.; use Eq. 1, 3):

$$\begin{aligned} \delta M_{z_1} &\overset{\rm oe1}{=} -h_{M_z}\,(1-\sin\psi_1\,\tfrac{9R_{\rm b}}{8H})\,\dot{x}_{\rm fa} + h_{M_z}\,\tilde{u}_1 + k_{M_z}\,\theta_1 \\ \delta M_{z_2} &\overset{\rm oe2}{=} -h_{M_z}\,(1-\sin\psi_2\,\tfrac{9R_{\rm b}}{8H})\,\dot{x}_{\rm fa} + h_{M_z}\,\tilde{u}_2 + k_{M_z}\,\theta_2 \\ \delta M_{z_3} &\overset{\rm oe3}{=} -h_{M_z}\,(1-\sin\psi_3\,\tfrac{9R_{\rm b}}{8H})\,\dot{x}_{\rm fa} + h_{M_z}\,\tilde{u}_3 + k_{M_z}\,\theta_3 \end{aligned} \tag{9}$$

Next to IPC, also control concepts apply for speed regulation, torsion damping and tower damping. The involved additional model output signals are the slow-shaft equivalent generator speed $\Omega_{\rm g}$ and the fore-aft and sideward tower speed $v_{\rm a}$ and $v_{\rm s}$:

$$\begin{aligned} \Omega_{\rm g} &\overset{\rm oe4}{=} \Omega_{\rm r} - \dot{\gamma} \\ v_{\rm a} &\overset{\rm oe5}{=} \dot{x}_{\rm fa} \\ v_{\rm s} &\overset{\rm oe6}{=} \dot{x}_{\rm sd} \end{aligned} \tag{10}$$

Although it is more realistic to assume that the fore-aft and sideward tower *acceleration* will be measured instead of the speed, it is more straightforward to use the speed signals from a conceptual point of view on control.

3 1P INDIVIDUAL PITCH CONTROL

In this study only a collective pitch feedback loop for speed regulation is added to the feedback loops for IPC-kp. The damping loops for the tower and drive-train are not considered here. The generator torque is tuned to the low-pass filtered rotor speed for rated power production.

In [2] is argued that the reduction of the (flap-wise) blade loading around the 1p-frequency can be achieved by low-frequency control of the so-called 'dq-axis loads'. The '1p'-blade flap loads become '0p'-tilt- and yaw-oriented loads in a dq-axis representation, which is commonly used in electric machine theory. The low-frequent 'dq-axis pitch actions' are transformed to '1p' true pitch actions.

It appears that both collective and 1p-individual pitch control can be derived from a same model for wind turbines with 3 blades or more. Such a model is obtained via the *multi-blade coordinate transformation* as proposed by Coleman and Feingold [4] of *all* model variables that are attached to the rotor blades; the feedback laws are then designed for the transformed model.

It is common use to apply the 'Coleman transformation' in the aeroelastic stability analysis [5] of wind turbines with polar symmetry ($\geq$3 blades): the rotating *state* variables are transformed. In our case also the rotating *input* and *output* variables are transformed; the resulting model is completely linear time-invariant.

The following three subsections deal with

- transformation of the control design model in multi-blade coordinates, the linear time-invariant *1p-transformed model*;
- design of the feedback laws for 1p-individual pitch control, combined with collective pitch control for speed regulation;
- extension of the IPC design approach to higher harmonics (IPC-2p and IPC-3p).

3.1 Linear time-invariant model

The equations of motion that depend on ψ from §2 do not include state variables attached to the blades or the rotor shaft except the rotational speed $\Omega_{\rm r}$ and shaft torsion γ. Since $\Omega_{\rm r}$ and γ have a co-axial orientation, not any state variable is to be transformed. The flapwise bending moments, pitch angles and blade effective wind speeds are the only variables to be transformed. When the corresponding variables on the three rotor blades are col-

lected in a coordinate vector $\underline{p}$, the Coleman transformation matrix $\boldsymbol{P}$ maps the multi-blade coordinates $\underline{p}_{\mathrm{cm}}$ to rotating coordinates in vector $\underline{p}$. With $\underline{\theta} = [\theta_1 \;\; \theta_2 \;\; \theta_3]'$, $\underline{\theta}_{\mathrm{cm}} = [\theta_{\mathrm{cm}_1} \;\; \theta_{\mathrm{cm}_2} \;\; \theta_{\mathrm{cm}_3}]'$, etc. it holds:

$$\underline{\theta} = \boldsymbol{P}\,\underline{\theta}_{\mathrm{cm}}\,, \quad \underline{\tilde{u}} = \boldsymbol{P}\,\underline{\tilde{u}}_{\mathrm{cm}}\,, \quad \delta\underline{M}_{z_{\mathrm{cm}}} = \boldsymbol{P}^{-1}\,\delta\underline{M}_z \tag{11}$$

with

$$\boldsymbol{P} = \begin{pmatrix} 1 & \sin\psi_1 & \cos\psi_1 \\ 1 & \sin\psi_2 & \cos\psi_2 \\ 1 & \sin\psi_3 & \cos\psi_3 \end{pmatrix}, \quad \boldsymbol{P}^{-1} = \begin{pmatrix} \frac{1}{3} & \frac{1}{3} & \frac{1}{3} \\ \frac{2}{3}\sin\psi_1 & \frac{2}{3}\sin\psi_2 & \frac{2}{3}\sin\psi_3 \\ \frac{2}{3}\cos\psi_1 & \frac{2}{3}\cos\psi_2 & \frac{2}{3}\cos\psi_3 \end{pmatrix} \tag{12}$$

It can be observed from figure 1 and the transformation with matrix $\boldsymbol{P}^{-1}$ that the 2nd and 3rd multi-blade flap moment coordinates $\delta M_{z_{\mathrm{cm}_2}}$ and $\delta M_{z_{\mathrm{cm}_3}}$ have a tilt- and yaw-orientation. The 1p-transformed model equations are obtained by carrying through the signal transformations by Eq. 11 in the periodic model of §2 ($B = 3$; Eq. 5, 7):

$$\begin{aligned}
J_{\mathrm{r}}\,\dot{\Omega}_{\mathrm{r}} &\overset{\mathrm{eom1}}{=} -s_{\mathrm{sh}}\,\gamma - d_{\mathrm{sh}}\,\dot{\gamma} - 3\,h_{M_x}\,\dot{x}_{\mathrm{fa}}\;\ldots \\
&\quad +3k_{M_x}\,\theta_{\mathrm{cm}_1} + 3h_{M_x}\,\tilde{u}_{\mathrm{cm}_1} \\
\tfrac{J_{\mathrm{r}}\,J_{\mathrm{g}}}{J_{\mathrm{r}}+J_{\mathrm{g}}}\,\ddot{\gamma} &\overset{\mathrm{eom2}}{=} -s_{\mathrm{sh}}\,\gamma - d_{\mathrm{sh}}\,\dot{\gamma} - \tfrac{J_{\mathrm{g}}}{J_{\mathrm{r}}+J_{\mathrm{g}}}\,3\,h_{M_x}\,\dot{x}_{\mathrm{fa}}\;\ldots \\
&\quad +\tfrac{J_{\mathrm{g}}}{J_{\mathrm{r}}+J_{\mathrm{g}}}\,3k_{M_x}\,\theta_{\mathrm{cm}_1} + \tfrac{J_{\mathrm{r}}}{J_{\mathrm{r}}+J_{\mathrm{g}}}\,\delta T_{\mathrm{g}} + \tfrac{J_{\mathrm{g}}}{J_{\mathrm{r}}+J_{\mathrm{g}}}\,3h_{M_x}\,\tilde{u}_{\mathrm{cm}_1} \\
m_{\mathrm{tw}}\,\ddot{x}_{\mathrm{fa}} &\overset{\mathrm{eom3}}{=} -s_{\mathrm{tw}}\,x_{\mathrm{fa}} - (d_{\mathrm{tw}} + 3h_{F_x} - \tfrac{81Rb}{32H^2}\,h_{M_z})\,\dot{x}_{\mathrm{fa}}\;\ldots \\
&\quad +3k_{F_x}\,\theta_{\mathrm{cm}_1} + \tfrac{9}{4H}k_{M_z}\theta_{\mathrm{cm}_2} + 3h_{F_x}\,\tilde{u}_{\mathrm{cm}_1} + \tfrac{9}{4H}h_{M_z}\,\tilde{u}_{\mathrm{cm}_2} \\
m_{\mathrm{tw}}\,\ddot{x}_{\mathrm{sd}} &\overset{\mathrm{eom4}}{=} -s_{\mathrm{tw}}\,x_{\mathrm{sd}} - d_{\mathrm{tw}}\,\dot{x}_{\mathrm{sd}} - \tfrac{27Rb}{16H}\,h_{F_z}\,\dot{x}_{\mathrm{fa}}\;\ldots \\
&\quad -\tfrac{3}{2}\,k_{F_z}\,\theta_{\mathrm{cm}_2} - \tfrac{3}{2}\,h_{F_z}\,\tilde{u}_{\mathrm{cm}_2} + \tfrac{3}{2H}\,\delta T_{\mathrm{g}}
\end{aligned} \tag{13}$$

and (Eq. 9; expressions for v_{fa} and v_{fa} omitted):

$$\begin{aligned}
\delta M_{z_{\mathrm{cm}_1}} &\overset{\mathrm{oe1}}{=} -h_{M_z}\,\dot{x}_{\mathrm{fa}} + k_{M_z}\,\theta_{\mathrm{cm}_1} + h_{M_z}\,\tilde{u}_{\mathrm{cm}_1} \\
\delta M_{z_{\mathrm{cm}_2}} &\overset{\mathrm{oe2}}{=} h_{M_z}\,\tfrac{9R_{\mathrm{b}}}{8H}\,\dot{x}_{\mathrm{fa}} + k_{M_z}\,\theta_{\mathrm{cm}_2} + h_{M_z}\,\tilde{u}_{\mathrm{cm}_2} \\
\delta M_{z_{\mathrm{cm}_3}} &\overset{\mathrm{oe3}}{=} k_{M_z}\,\theta_{\mathrm{cm}_3} + h_{M_z}\,\tilde{u}_{\mathrm{cm}_3} \\
\Omega_{\mathrm{g}} &\overset{\mathrm{oe4}}{=} \Omega_{\mathrm{r}} - \dot{\gamma}
\end{aligned} \tag{14}$$

The equations of motion for Ω_{r}, γ and x_{fa} show that the 1st multi-blade pitch angle coordinate θ_{cm_1} represents collective pitching; this can also be concluded from the transformation of θ_{cm_1} with matrix $\boldsymbol{P}$ to contributions to θ_1, θ_2 and θ_3. The output equations for $\delta M_{z_{\mathrm{cm}_2}}$ and $\delta M_{z_{\mathrm{cm}_3}}$ show that the 2nd and 3rd multi-blade pitch angle coordinates θ_{cm_2} and θ_{cm_3} have also a tilt and yaw orientation.

The use of this time-invariant 1p-transformed model is identical to the use of the periodic model of §2 if

- blade input variables are demodulated before they enter the 1p-transformed model:

$$\underline{\theta}_{\mathrm{cm}} = \boldsymbol{P}^{-1}\,\underline{\theta}\,, \quad \underline{\tilde{u}}_{\mathrm{cm}} = \boldsymbol{P}^{-1}\,\underline{\tilde{u}}\,,$$

- blade output variables are remodulated after they have left the 1p-transformed model:

$$\delta\underline{M}_z = \boldsymbol{P}\,\delta\underline{M}_{z_{\mathrm{cm}}}$$

This approach can be applied to any linear time invariant state space model for polar-symmetric wind turbines ($B \geq 3$), like the one used in [11] .

3.2 Feedback laws for IPC-1p

The layout of the feedback loops for rotor speed regulation and blade load reduction around 1p is pictured below.

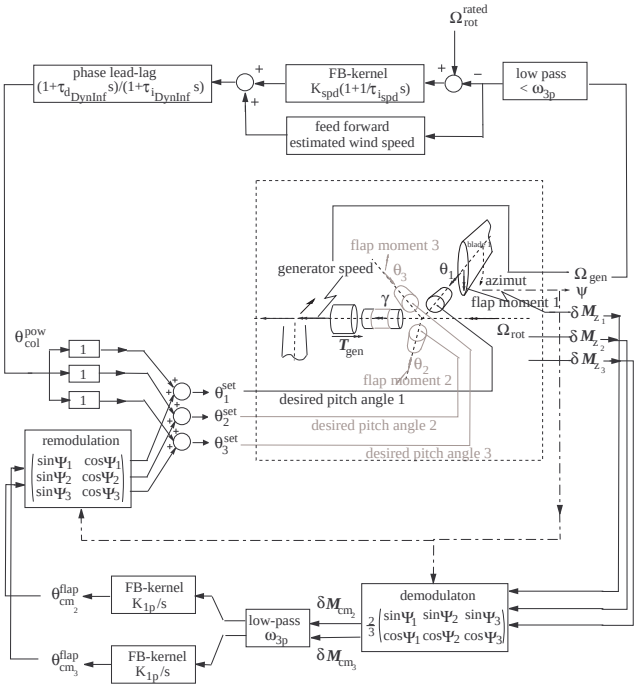

Figure 2: *Layout of control loops for pitch control*

The feedback loops map

- the low-pass filtered rotational speed Ω_{g} to the collective pitch angle setpoint $\theta_{\mathrm{col}}^{\mathrm{pow}}$ via a proportional/integral scheme (PI-compensator), enforced by 'feedforward' of the estimated wind speed while catering for dynamic inflow effects.
- the identically low-pass filtered tilt- and yaw-oriented multi-blade flap moment coordinates $\delta M_{z_{\mathrm{cm}_2}}$ and $\delta M_{z_{\mathrm{cm}_3}}$ to the tilt- and yaw-oriented multi-blade pitch angle coordiates θ_{cm_2} and θ_{cm_3} via equal integral gains (I-compensator).

The latter implies the following (1p-demodulating) creation scheme for the 'artificial measurement signals' $\delta M_{z_{\mathrm{cm}_2}}$ and $\delta M_{z_{\mathrm{cm}_3}}$ (further referred to as $\delta M^{(1)}_{z_{\mathrm{cm}_2}}$ and $\delta M^{(1)}_{z_{\mathrm{cm}_3}}$ since they pertain to IPC-1p):

$$\begin{bmatrix} \delta M^{(1)}_{z_{\mathrm{cm}_2}} \\ \delta M^{(1)}_{z_{\mathrm{cm}_3}} \end{bmatrix} = \begin{bmatrix} \frac{2}{3}\sin\psi_1 & \frac{2}{3}\sin\psi_2 & \frac{2}{3}\sin\psi_3 \\ \frac{2}{3}\cos\psi_1 & \frac{2}{3}\cos\psi_2 & \frac{2}{3}\cos\psi_3 \end{bmatrix} \begin{pmatrix} \delta M_{z_1} \\ \delta M_{z_2} \\ \delta M_{z_3} \end{pmatrix} \tag{15}$$

while pitch angle additions around the 1p frequency are obtained via a 1p-modulation scheme on the 'ar-

tificial control signals' θ_{cm_2} and θ_{cm_3} $(= \theta^{(1)}_{\mathrm{cm}_2}, \theta^{(1)}_{\mathrm{cm}_3})$:

$$\begin{bmatrix} \theta^{(1)}_1 \\ \theta^{(1)}_2 \\ \theta^{(1)}_3 \end{bmatrix} = \begin{pmatrix} \sin\psi_1 & \cos\psi_1 \\ \sin\psi_2 & \cos\psi_2 \\ \sin\psi_3 & \cos\psi_3 \end{pmatrix} \begin{bmatrix} \theta^{(1)}_{\mathrm{cm}_2} \\ \theta^{(1)}_{\mathrm{cm}_3} \end{bmatrix} \tag{16}$$

The model equations below are derived from the 1p-transformed model and are used for the parametrisation of the three pitch feedback loops (delay τ_{v} models all dynamics of measuring, data processing and pitch actuation; use Eq. 13, 14; drive-train torsion and tower fore-aft motion excluded):

$$\begin{aligned} (J_{\mathrm{r}} + J_{\mathrm{g}})\,\dot{\Omega}_{\mathrm{g}}(t) &= 3\,k_{M_x}\,\theta_{\mathrm{cm}_1}(t-\tau_{\mathrm{v}}) + 3\,h_{M_x}\,\tilde{u}_{\mathrm{cm}_1}(t) \\ \delta M_{\mathrm{cm}_2}(t) &= k_{M_z}\,\theta_{\mathrm{cm}_2}(t-\tau_{\mathrm{v}}) + h_{M_z}\,\tilde{u}_{\mathrm{cm}_2}(t) \\ \delta M_{\mathrm{cm}_3}(t) &= k_{M_z}\,\theta_{\mathrm{cm}_3}(t-\tau_{\mathrm{v}}) + h_{M_z}\,\tilde{u}_{\mathrm{cm}_3}(t) \end{aligned} \tag{17}$$

These equations are completely decoupled so that pure single-input/single-output (SISO) control theory can be applied. As argued in the begin of §3, the 1p-load reduction objective is satisfied by zeroing the tilt- and yaw-oriented multi-blade flap moment coordinates M_{cm_2} and M_{cm_3}. Thus, three so called SISO 'regulator problems' are to be solved.

The PI-compensator is commonly used as the basic feedback law for regulation of a system characterised by a delayed integrator, which applies in the speed regulation loop [6] . The cut-off frequency loop must lay below 3p in order to avoid the feedthrough of rotor-wide rotational sampling effects ($\tilde{u}_{\mathrm{cm}_1} = \tilde{u}_1 + \tilde{u}_2 + \tilde{u}_3$), which occur around (multiples of) the 3p-frequency. The lead-lag filter is derived for the compensation of dynamic inflow at collective pitching [7] . The estimated wind speed $\hat{V}_{\mathrm{w}}$ is fed forward to a pitch angle value that corresponds to rated power capture in $\hat{V}_{\mathrm{w}}$ [8] .

The load regulation loops actually behave as a delayed proportional system. In that case just an I-compensator satisfies for regulation and thus IPC-1p. In these loops it is also required to filter out the signal contents around and beyond 3p. This becomes clear when the multi-blade wind speed coordinates $\tilde{u}_{\mathrm{cm}_2}$ and $\tilde{u}_{\mathrm{cm}_3}$ are decomposed in rotational modes.

For homogeneous turbulence in the rotor plane, a *time-dependent* Fourier expansion of the wind speed $\tilde{u}_i$ experienced in a rotating point on radius r exists [9] :

$$\tilde{u}_i(t) = \sum_{p=-\infty}^{\infty} \mathrm{e}^{\jmath p\psi_i}\,\hat{u}_p(t), \quad \hat{u}_p(t) = \tfrac{1}{2\pi}\int_0^{2\pi} \mathrm{e}^{-\jmath p\phi}\,u(t,r,\phi)\,\mathrm{d}\phi \tag{18}$$

The Fourier coefficients $\hat{u}_p(t)$, the *rotational modes*, are time-dependent. A rotational mode is a harmonic basis function over the circle on radius r of the wind field. The time-dependency represents the evolution of the amplitude and the phase of such a rotational mode, which mainly occurs in frequencies below 0.1Hz[1]. For the multi-blade coordinates $\tilde{u}_{\mathrm{cm}_2}$ and $\tilde{u}_{\mathrm{cm}_3}$ then holds (use row 2 and 3 of $\boldsymbol{P}^{-1}$ by Eq. 12 and see App. A for $k = 1$):

$$\begin{aligned} \tilde{u}_{\mathrm{cm}_2}(t) &= \sum_{m=-\infty}^{\infty} \jmath\,\mathrm{e}^{\jmath 3m\psi}(\,\hat{u}_{3m+1}(t) - \hat{u}_{3m-1}(t)\,) \\ \tilde{u}_{\mathrm{cm}_3}(t) &= \sum_{m=-\infty}^{\infty} \mathrm{e}^{\jmath 3m\psi}(\,\hat{u}_{3m+1}(t) + \hat{u}_{3m-1}(t)\,) \end{aligned} \tag{19}$$

These expressions tell that the rotational mode pair $\{\hat{u}_1, \hat{u}_{-1}\}$ contributes straightforward to $\tilde{u}_{\mathrm{cm}_2}$ and $\tilde{u}_{\mathrm{cm}_3}$ while the mode pairs $\{\hat{u}_2, \hat{u}_4\}$ and $\{\hat{u}_{-2}, \hat{u}_{-4}\}$ deliver contributions that are modulated with the 3p-frequency. Similarly, the pairs $\{\hat{u}_5, \hat{u}_7\}$ and $\{\hat{u}_{-5}, \hat{u}_{-7}\}$ yield 6p-modulated contributions.

It is clear that the integral action in the feedback loops compensate for the low frequent variations in the modes $\{\hat{u}_1, \hat{u}_{-1}\}$ as well as for the mean-value parts associated with tower shadow and wind shear, and thus realises IPC-1p. The pursued bandwidth of the feedback loop amounts to ca. 0.1 Hz. In order to prevent the influence of higher harmonics in IPC-1p it is required to apply low pass filtering around and beyond 3p.

IPC-1p can thus be realised by solving a regulator problem. The receipt is:

- transform the three flapwise blade root moments δM_{z_i} into artificial '1p-demodulated' measurement signals $\delta M^{(1)}_{z_{\mathrm{cm}_2}}$ and $\delta M^{(1)}_{z_{\mathrm{cm}_3}}$ by Eq. 15;
- generate artificial control signals $\theta^{(1)}_{\mathrm{cm}_2}$ and $\theta^{(1)}_{\mathrm{cm}_3}$ via I-compensators for $\delta M^{(1)}_{z_{\mathrm{cm}_2}}$ and $\delta M^{(1)}_{z_{\mathrm{cm}_3}}$ with low pass filters around and beyond 3p;
- transform $\theta^{(1)}_{\mathrm{cm}_2}$ and $\theta^{(1)}_{\mathrm{cm}_3}$ into three '1p-modulated' pitch signals $\theta^{(1)}_i$ by Eq. 16.

3.3 Higher harmonics control

The approach described for 1p individual pitch control is also adopted for load reduction in the rotor blades around the 2p-frequency and the 3p-frequency (IPC-2p and IPC-3p). It appears that higher harmonics control can also be realised via regulator problems.

Feedback loops for IPC-2p
We assumed that pitch angle additions for IPC-**2**p could be obtained from low-frequent artificial control signals $\theta^{(2)}_{\mathrm{cm}_2}$ and $\theta^{(2)}_{\mathrm{cm}_3}$. These are related to the pitch angle variations $\theta^{(2)}_1$, $\theta^{(2)}_2$ and $\theta^{(2)}_3$ by:

$$\begin{bmatrix} \theta^{(2)}_1 \\ \theta^{(2)}_2 \\ \theta^{(2)}_3 \end{bmatrix} = \begin{pmatrix} \sin 2\psi_1 & \cos 2\psi_1 \\ \sin 2\psi_2 & \cos 2\psi_2 \\ \sin 2\psi_3 & \cos 2\psi_3 \end{pmatrix} \begin{bmatrix} \theta^{(2)}_{\mathrm{cm}_2} \\ \theta^{(2)}_{\mathrm{cm}_3} \end{bmatrix} \tag{20}$$

This 2p-modulation scheme was carried through in the periodic linear model of §2 and yielded the *2p-transformed model*. It appeared that these pitching actions affect neither the aerodynamic torque T_{a} nor the axial force F_{a}, tilt moment M_{t} and sideward force F_{s}. Thus, the system dynamics are not excited at all by the proposed 2p pitch angle additions.

[1] In a linearised approach, tower shadow and wind shear can be considered as the mean-value part of the rotational modes

The i^{th} blade flap moment is affected as follows by $\theta^{(2)}_{\text{cm}_2}$ and $\theta^{(2)}_{\text{cm}_3}$ (see Eq. 9):

$$\begin{aligned}\delta M_{z_i} = -h_{M_z}\,(1-\sin\psi_i\,\tfrac{9R_\text{b}}{8H})\,\dot{x}_\text{fa} + h_{M_z}\,\tilde{u}_i + \\ k_{M_z}\,(\sin 2\psi_i\,\theta^{(2)}_{\text{cm}_2} + \cos 2\psi_i\,\theta^{(2)}_{\text{cm}_3})\end{aligned} \tag{21}$$

For the artificial measurement signals $\delta M^{(2)}_{z_{\text{cm}_2}}$ and $\delta M^{(2)}_{z_{\text{cm}_3}}$, obtained as:

$$\begin{bmatrix}\delta M^{(2)}_{z_{\text{cm}_2}} \\ \delta M^{(2)}_{z_{\text{cm}_3}}\end{bmatrix} = \begin{bmatrix}\frac{2}{3}\sin 2\psi_1 & \frac{2}{3}\sin 2\psi_2 & \frac{2}{3}\sin 2\psi_3 \\ \frac{2}{3}\cos 2\psi_1 & \frac{2}{3}\cos 2\psi_2 & \frac{2}{3}\cos 2\psi_3\end{bmatrix}\begin{pmatrix}\delta M_{z_1} \\ \delta M_{z_2} \\ \delta M_{z_3}\end{pmatrix} \tag{22}$$

then holds:

$$\begin{aligned}\delta M^{(2)}_{z_{\text{cm}_2}} &= k_{M_z}\,\theta^{(2)}_{\text{cm}_2} + h_{M_z}\,\tfrac{2}{3}\sum_{i=1}^{B}\sin 2\psi_i\,\tilde{u}_i \\ \delta M^{(2)}_{z_{\text{cm}_3}} &= k_{M_z}\,\theta^{(2)}_{\text{cm}_3} + h_{M_z}\,\tfrac{2}{3}\sum_{i=1}^{B}\cos 2\psi_i\,\tilde{u}_i\end{aligned} \tag{23}$$

When the rotational mode expansion by Eq. 18 is carried through in these expressions, the following appears:

- rotational mode pair $\{\hat{u}_2, \hat{u}_{-2}\}$ contributes proportionally to $\delta M^{(2)}_{z_{\text{cm}_2}}$ and $\delta M^{(2)}_{z_{\text{cm}_3}}$;
- remaining mode pairs deliver contributions that are modulated with (multiples of) 3p.

It is clear that integral action in the feedback loops from $\delta M^{(2)}_{z_{\text{cm}_2}}$ and $\delta M^{(2)}_{z_{\text{cm}_3}}$ to $\theta^{(2)}_{\text{cm}_2}$ and $\theta^{(2)}_{\text{cm}_3}$ will compensate for the low frequency contents of the mode-pair $\{\hat{u}_2, \hat{u}_{-2}\}$.

Thus, the same receipt as listed at the end of §3 is valid for IPC-2p. Low pass filtering around and beyond 3p is now required against excitation from mode-pairs $\{\hat{u}_{\pm 5}, \hat{u}_{\pm 1}\}$, $\{\hat{u}_{\pm 8}, \hat{u}_{\pm 4}\}$, etc.

Feedback loops for IPC-3p

Just as for IPC-2p, we defined artificial control signals $\theta^{(3)}_{\text{cm}_2}$ and $\theta^{(3)}_{\text{cm}_3}$ for IPC-3p, but now with a 3p-modulation scheme:

$$\begin{bmatrix}\theta^{(3)}_1 \\ \theta^{(3)}_2 \\ \theta^{(3)}_3\end{bmatrix} = \begin{pmatrix}\sin 3\psi_1 & \cos 3\psi_1 \\ \sin 3\psi_2 & \cos 3\psi_2 \\ \sin 3\psi_3 & \cos 3\psi_3\end{pmatrix}\begin{bmatrix}\theta^{(3)}_{\text{cm}_2} \\ \theta^{(3)}_{\text{cm}_3}\end{bmatrix} \tag{24}$$

This scheme was carried through in the periodic linear model of §2 and yielded the *3p-transformed model*. The '3p'-pitching actions *do* affect the aerodynamic torque T_a and axial force F_a but *do not* affect the tilt moment M_t and sideward force F_s.

The i^{th} blade flap moment is affected as follows by $\theta^{(3)}_{\text{cm}_2}$ and $\theta^{(3)}_{\text{cm}_3}$ (see Eq. 9):

$$\begin{aligned}\delta M_{z_i} = -h_{M_z}\,(1-\sin\psi_i\,\tfrac{9R_\text{b}}{8H})\,\dot{x}_\text{fa} + h_{M_z}\,\tilde{u}_i + \\ k_{M_z}\,(\sin 3\psi_i\,\theta^{(3)}_{\text{cm}_2} + \cos 3\psi_i\,\theta^{(3)}_{\text{cm}_3})\end{aligned} \tag{25}$$

For the artificial measurement signals $\delta M^{(3)}_{z_{\text{cm}_2}}$ and $\delta M^{(3)}_{z_{\text{cm}_3}}$, obtained as:

$$\begin{bmatrix}\delta M^{(3)}_{z_{\text{cm}_2}} \\ \delta M^{(3)}_{z_{\text{cm}_3}}\end{bmatrix} = \begin{bmatrix}\frac{2}{3}\sin 3\psi_1 & \frac{2}{3}\sin 3\psi_2 & \frac{2}{3}\sin 3\psi_3 \\ \frac{2}{3}\cos 3\psi_1 & \frac{2}{3}\cos 3\psi_2 & \frac{2}{3}\cos 3\psi_3\end{bmatrix}\begin{pmatrix}\delta M_{z_1} \\ \delta M_{z_2} \\ \delta M_{z_3}\end{pmatrix} \tag{26}$$

then holds:

$$\begin{aligned}\delta M^{(3)}_{z_{\text{cm}_2}} &= -2h_{M_z}\,\sin 3\psi\,\tfrac{9R_\text{b}}{8H}\,\dot{x}_\text{fa} + h_{M_z}\,\tfrac{2}{3}\sum_{i=1}^{3}\sin 3\psi_i\,\tilde{u}_i + \\ &\quad k_{M_z}\,(\,\theta^{(3)}_{\text{cm}_2} - \cos 6\psi\,\theta^{(3)}_{\text{cm}_2} + \sin 6\psi\,\theta^{(3)}_{\text{cm}_3}\,) \\ \delta M^{(3)}_{z_{\text{cm}_3}} &= -2h_{M_z}\,\sin 3\psi\,\tfrac{9R_\text{b}}{8H}\,\dot{x}_\text{fa} + h_{M_z}\,\tfrac{2}{3}\sum_{i=1}^{3}\cos 3\psi_i\,\tilde{u}_i + \\ &\quad k_{M_z}\,(\,\theta^{(3)}_{\text{cm}_3} + \cos 6\psi\,\theta^{(3)}_{\text{cm}_3} + \sin 6\psi\,\theta^{(3)}_{\text{cm}_2}\,)\end{aligned} \tag{27}$$

It can now be proved that the rotational mode pair $\{\hat{u}_3, \hat{u}_{-3}\}$ proportionally contributes to $\delta M^{(3)}_{z_{\text{cm}_2}}$ and $\delta M^{(3)}_{z_{\text{cm}_3}}$ while the remaining mode pairs deliver contributions that are modulated with (multiples of) 3p.

Integral action in the feedback loops from $\delta M^{(3)}_{z_{\text{cm}_2}}$ and $\delta M^{(3)}_{z_{\text{cm}_3}}$ to $\theta^{(3)}_{\text{cm}_2}$ and $\theta^{(3)}_{\text{cm}_3}$ will now compensate for the mode-pair $\{\hat{u}_3, \hat{u}_{-3}\}$. Low pass filtering is required around and beyond 3p in order to avoid undesired feedback that is caused by:

- mode-pairs $\{\hat{u}_{\pm 6}, \hat{u}_{\pm 0}\}$, $\{\hat{u}_{\pm 9}, \hat{u}_{\pm 12}\}$, etc.;
- 6p-modulated terms like $-k_{M_z}\cos 6\psi\,\theta^{(3)}_{\text{cm}_2}$;
- 3p-modulated term $-2h_{M_z}\,\sin 3\psi\,\tfrac{9R_\text{b}}{8H}\,\dot{x}_\text{fa}$.

4 TIME DOMAIN SIMULATION

Time-domain simulations were performed with the controlled model. These were driven by the *blade effective* wind input signals as mentioned in §2. Four cases were addressed:

- collective pitch only;
- collective pitch and IPC-1p;
- collective pitch and IPC-1p, IPC-2p;
- collective pitch and IPC-1p, IPC-2p, IPC-3p.

The model parameters pertain to a typcial 3MW wind turbine with 45m rotor radius R_b, 70 m tower height H, overall drive-train inertia $J_\text{r} + J_\text{g}$ of $12 \cdot 10^6$ kgm^2, and the 1$^{\text{st}}$ tower eigenfrequency to 0.35 Hz. The parameters were determined for a wind speed of 16 m/s, rotor speed to 15 rpm and pitch angle of 10$^\text{o}$. Parasiticals dynamics by pitch actuation, sensororing and data processing were catered for via an overall loop delay of 0.2 s.

Each box in the following figures always contains the results for collective pitch control only as a blue (dark) line. The results with any individual pitch control included are plotted as a green (light) line.

Figure 3 shows realisations and power spectra of the blade root flap moment and the tilt moment in the rotor centre. The three boxes with realisations for a signal pertain to different levels of activity of individual pitch control; the upper box includes results for IPC-1p, the middle box for combined IPC-1p and IPC-2p, and the lower for combined IPC-1p, IPC-2 and IPC-3. The three boxes with auto power spectra for a signals represent these IPC-activity levels from left to right.

The graphs show the respective reduction of blade loads around 1p, 2p and 3p and of tilt loads in very

low frequency and around 3p; the latter is caused by the reduction of blade flap loads around 2p. The yaw moment looked similar to the tilt moment.

Fatigue damage reduction estimations were derived via rainflow counting on 6 simulations of more than 10 minutes. The loads were transformed into 1Hz equivalent fatique loads and mapped to fatigue damage via the method of Palmgren and Miner [12] . The achieved reduction in fatigue damage is shown for different values of the slope m (3 or 4 for steel; 9 or 10 for for reinforced plastics).

Fatigue damage reduction up to 20 to 30% in frequently occurring full load conditions seems realistic. About one third is obtained from IPC-2p and IPC-3p. The fatigue damage reduction of the nacelle is almost completely obtained from IPC-2p.

It appeared that the required maximum pitch speed rises from ca. 2 ^{o}/s at collective pitch only, via 7^o/s and 10^o/s at IPC-1p and IPc-2 up to 12^o/s at IPC-3p. The respective pitch acceleration maxima are ca 3^o/s^2, 18^o/s^2, 27^o/s^2 and 50 ^{o}/s^2. The fore-aft tower motion is somewhat raised by IPC-1p. This is caused by the presence of pitch coordinate $\theta^{(1)}_{\mathrm{cm}_2}$ in the equation of motion for $\dot{x}_{\mathrm{fa}}$ (see Eq. 13.

5 CONCLUSION

A simple design model has been derived via a multi-blade transformation for the design of both rotor speed regulation and 1p individual pitch control. Basic scalar control theory can be applied (phase and gain margins).

The adopted approach has been extended to multiples of the rotational frequency (IPC-2p, IPC-3p). Now multi-blade transformations in two and three times the blade azimut angles apply. Similar scalar control design appeared to be valid. Especially IPC-2p is very straightforward with a beneficial effect on 3p tilt and yaw loading.

Preliminary time-domain simulations in full load conditions predict an achievable reduction in fatigue damage of up to 20 to 30% in both the blade loads and the nacelle loads.

It is recommended to

- explicitely clarify the working of IPC via the decomposition of the sampled wind field by the rotor blades in rotational modes;
- include blade bending and unsteady aerodynamics in the approach;
- formulate a linear model with feedback loops for IPC-kp included for overall stability assessment;
- to develop a procedure for stability assessment based on the proposed integral model formulation and Floquet theory [13] .

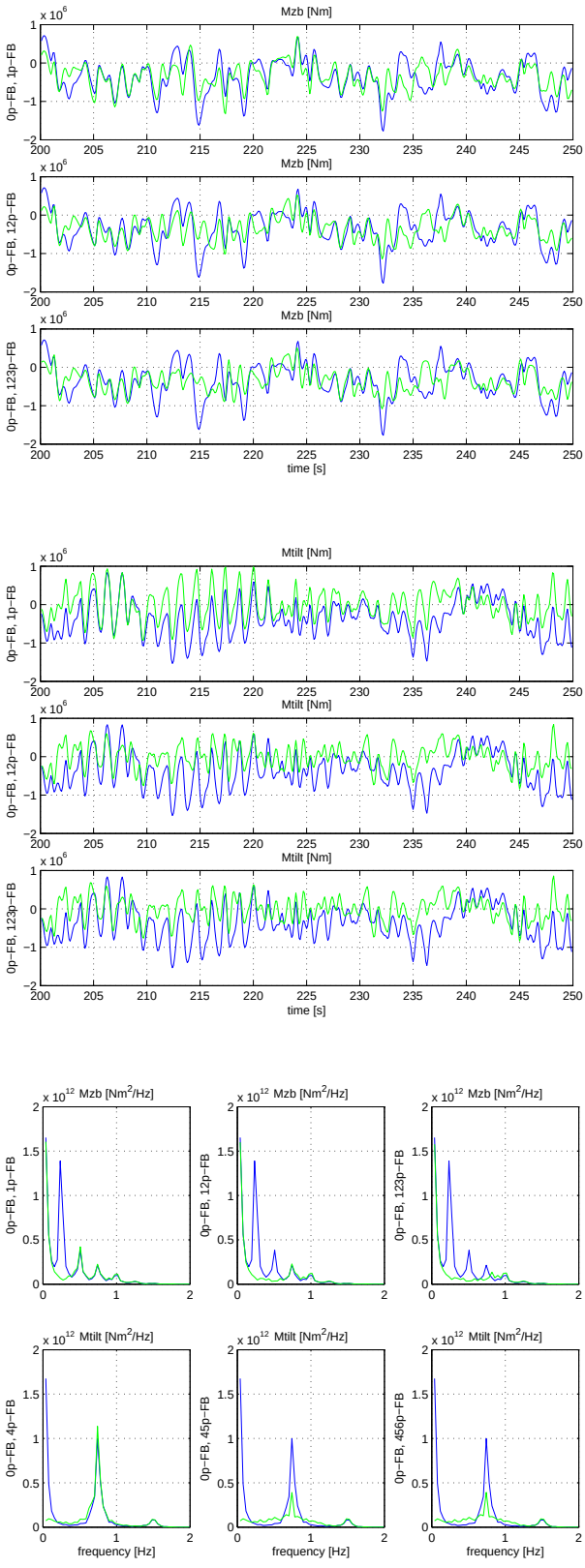

Figure 3: *Realisations and power spectra for the blade root flap moment (Mzb) and the tilt moment in the rotor centre (Mtilt) in 16 m/s*

ACKNOWLEDGEMENT

A very preliminary elaboration of multi-rotational mode individual pitch control (IPC-kp) has been carried out in the project 'Ontwerpgereedschap voor Windturbine Regelingen' (Dutch DEN program supported by SenterNovem, an agency of the Dutch Ministry of Economic Affairs under grant 2020-01-12-10-003 [10])). The approach to IPC-1p via the multi-blade transformation by Coleman was part of the European Union project StabCon (5^{th} Framework supported by the EU and SenterNovem under grant ENK5-CT-2002-00627 [3]).
Eric van der Hooft (ECN) is acknowlegded for co-reading and useful recommendations.

REFERENCES

[1] P. Caselitz, W. Kleinkauf, W. Krueger, J. Petschenka, M. Reichardt, K Stoerzel, *Reduction of fatigue loads on wind energy converters by advanced control methods*; in Proceedings European Wind Energy Conference, Dublin, 555-558, Irish Wind Eenrgy Association, 1997.

[2] E.A. Bossanyi, *Developments in Individual Blade Pitch Control*; in Proceedings of special topic conference on the Science of Making Torque from Wind, pp. 486-497, Delft, the Netherlands, April 2004

[3] T.G. van Engelen, D. Winkelaar, H. Markou (Risø), T. Buhl (Risø), B. Marrant (TU Delft), *Morphological Study of Aeroelastic Control Concepts for Wind Turbines, StabCon Task-7 Report*, ¡to be published in May 2006¿, ECN Wind Energy, Petten, the Netherlands

[4] R.P. Coleman, A.M. Feingold, *Theory of Self-Excited Mechanical Oscillations of Helicopter Rotors with Hinged Blades*, NASA-TN 3844, NASA, 1957.

[5] M.H. Hansen, *Aeroelastic Stability Analysis of Wind Turbines Using an Eigenvalue Approach*, in Proceedings of European Wind Energy Conference in Madrid, Spain, 2003

[6] T.G. van Engelen, E.L. van der Hooft, P. Schaak, *Development of Wind Turbine Control Algorithms for Industrial Usage*; in Proceedings of European Wind Energy Conference in Copenhagen, Danmark, 2001.

[7] T.G. van Engelen, E.L. van der Hooft, *Dynamic Inflow Compensation for Pitch Controlled Wind Turbines*; in Proceedings of European Wind Energy Conference in London, UK, 2004.

[8] E.L. van der Hooft, T.G. van Engelen, *Estimated Wind Speed Feed Forward Control for Wind Turbine Operation Optimisation*; in Proceedings of European Wind Energy Conference in London, UK, 2004.

[9] J.B. Dragt, *Atmospheric Turbulence Characteristics in the Rotating Frame of Reference of a WECS Rotor*; in Proceedings of European Wind Energy Conference in Madrid, Spain, 1990.

[10] T.G. van Engelen, E.L. van der Hooft, *Individual Pitch Control, Inventory*; Technical Report ECN-C–03-138, ECN Wind Energy, ECN Petten, the Netherlands.

[11] T.G. van Engelen, H. Braam, *TURBU Offshore, Computer Program for Frequency Domain Analysis of Horizontal Axis Offshore Wind Turbines; Implementation*; Technical Report ECN-C–04-079, ECN Wind Energy, ECN Petten, the Netherlands.

[12] M.A. Miner, *Cumulative damage in fatigue*; in Journal of Applied Mechanics, 12:159-164, 1945

[13] V.A. Yakubovich, V.M. Starzhinskii, *Linear Differential Equations with Periodic Coefficients*, John Wiley and Sons, Inc., New York, 1975.

A Rotational mode expansions

Expressions are listed for multi-blade wind speed coordinates in the rotational modes $\{\hat{u}_p\}$ of the wind speed as experienced on corresponding blade locations of a 3-bladed rotor ($\tilde{u}_1$, $\tilde{u}_2$ and $\tilde{u}_3$). The multi-blade coordinates $\tilde{u}^{(k)}_{\text{cm}_1}$, $\tilde{u}^{(k)}_{\text{cm}_2}$ and $\tilde{u}^{(k)}_{\text{cm}_3}$ are related to $\tilde{u}_1$, $\tilde{u}_2$ and $\tilde{u}_3$ by:

$$\begin{bmatrix} \tilde{u}^{(k)}_{\text{cm}_1} \\ \tilde{u}^{(k)}_{\text{cm}_2} \\ \tilde{u}^{(k)}_{\text{cm}_3} \end{bmatrix} = \begin{pmatrix} \frac{1}{3} & \frac{1}{3} & \frac{1}{3} \\ \frac{2}{3}\sin k\psi_1 & \frac{2}{3}\sin k\psi_2 & \frac{2}{3}\sin k\psi_3 \\ \frac{2}{3}\cos k\psi_1 & \frac{2}{3}\cos k\psi_2 & \frac{2}{3}\cos k\psi_3 \end{pmatrix} \begin{bmatrix} \tilde{u}_1 \\ \tilde{u}_2 \\ \tilde{u}_3 \end{bmatrix} \tag{28}$$

With rotor azimut ψ equal to the azimut ψ_1 of the first blade it holds:

$$\begin{aligned} \tilde{u}^{(k)}_{\text{cm}_1} &= \tfrac{1}{3}\sum_{p=-\infty}^{\infty}\sum_{i=1}^{3}(\cos p\psi_i + \jmath \sin p\psi_i)\,\hat{u}_p \\ &= \tfrac{1}{3}\sum_{p=-\infty}^{\infty}\sum_{i=1}^{3}\mathrm{e}^{\jmath(p)\psi_i}\,\hat{u}_p \\ &= \tfrac{1}{3}\sum_{m=-\infty}^{\infty} 3\,\mathrm{e}^{\jmath 3m\psi}\hat{u}_{3m} \end{aligned} \tag{29}$$

$$\begin{aligned} \tilde{u}^{(k)}_{\text{cm}_2} &= \tfrac{2}{3}\sum_{p=-\infty}^{\infty}\sum_{i=1}^{3}(\cos p\psi_i + \jmath \sin p\psi_i)\,\sin k\psi_i\,\hat{u}_p \\ &= \tfrac{1}{3}\sum_{p=-\infty}^{\infty}\sum_{i=1}^{3}(\sin(p+k)\psi_i - \sin(p-k)\psi_i \\ &\qquad -\jmath\cos(p+k)\psi_i + \jmath\cos(p-k)\psi_i)\,\hat{u}_p \\ &= \tfrac{1}{3}\sum_{m=-\infty}^{\infty} 3\,\jmath\,\mathrm{e}^{\jmath 3m\psi}(\,\hat{u}_{3m+k} - \hat{u}_{3m-k}\,) \end{aligned} \tag{30}$$

$$\begin{aligned} \tilde{u}^{(k)}_{\text{cm}_3} &= \tfrac{2}{3}\sum_{p=-\infty}^{\infty}\sum_{i=1}^{3}(\cos p\psi_i + \jmath \sin p\psi_i)\,\cos k\psi_i\,\hat{u}_p \\ &= \tfrac{1}{3}\sum_{p=-\infty}^{\infty}\sum_{i=1}^{3}(\cos(p+k)\psi_i + \cos(p-k)\psi_i \\ &\qquad +\jmath\sin(p+k)\psi_i + \jmath\sin(p-k)\psi_i)\,\hat{u}_p \\ &= \tfrac{1}{3}\sum_{m=-\infty}^{\infty} 3\,\mathrm{e}^{\jmath 3m\psi}(\,\hat{u}_{3m+k} + \hat{u}_{3m-k}\,) \end{aligned} \tag{31}$$